# Active site profiling reveals coupling between domains in SRC-family kinases

**Ratika Krishnamurty**[1], **Jennifer L. Brigham**[1], **Stephen E. Leonard**[1], **Pratistha Ranjitkar**[1], **Eric T. Larson**[2], **Edward J. Dale**[1], **Ethan A. Merritt**[2], and **Dustin J. Maly**[1,*]

[1]Department of Chemistry, University of Washington. Seattle, WA 98195. U.S.A.

[2]Department of Biochemistry, University of Washington. Seattle, WA 98195. U.S.A.

## Abstract

Protein kinases, key regulators of intracellular signal transduction, have emerged as an important class of drug targets. Chemical proteomic tools that facilitate the functional interrogation of protein kinase active sites are powerful reagents for studying the regulation of this large enzyme family and for performing inhibitor selectivity screens. Here we describe a new crosslinking strategy that enables rapid and quantitative profiling of protein kinase active sites in lysates and live cells. Applying this methodology to the SRC-family kinases (SFKs) SRC and HCK led to the identification of a series of conformation-specific, ATP-competitive inhibitors that display a distinct preference for autoinhibited forms of these kinases. Furthermore, we show that ligands that demonstrate this selectivity are able to modulate the ability of the regulatory domains of SRC and HCK to engage in intermolecular binding interactions. These studies provide insight into the regulation of this important family of tyrosine kinases.

Protein kinases are a large family of enzymes that mediate intracellular protein phosphorylation[1]. Spatial and temporal coordination of protein kinase activity is essential for proper cellular function. Therefore, it is not surprising that protein kinase misregulation leads to a variety of diseases including cancer, inflammation, and diabetes[2]. A correspondingly large percentage of drug discovery research focuses on kinase inhibitors as molecularly targeted drugs, with over a dozen successfully completing clinical trials[3]. Significant efforts have been made to investigate this large enzyme family, of which only a small percentage of its 518 members have been functionally analyzed. The functional annotation of enzymes in other large protein families has greatly benefited from the development of activity- and affinity-based probes that selectively target conserved active site features[4,5]. For example, activity-based fluorophosphonate probes have proven to be

powerful reagents for uncovering potential new serine hydrolase drug targets and performing inhibitor selectivity screens in complex proteomes[6]. While a number of useful proteomic tools have been developed for studying protein kinases[7–9], there remains a need for reagents that allow rapid and quantitative analysis of protein kinase active sites in their native biological environments.

In order to comprehensively profile the roles that protein kinases play in the cell, methods that facilitate interrogation of their ATP-binding sites irrespective of their functional or activation state are particularly useful. In this study, we detail the development and application of a new method for the intracellular labeling of protein kinases in complex biological mixtures. Our strategy relies on a cell-permeable, ATP-competitive photo-probe that covalently modifies the ATP-binding sites of protein kinases upon irradiation with ultraviolet (UV) light. This probe contains an orthogonal chemical handle that facilitates the rapid and quantitative profiling of protein kinase active sites in their native biological environments.

In this study, we have applied our labeling strategy to a family of multidomain, nonreceptor tyrosine kinases called the SRC-family kinases (SFKs). These kinases play important roles in mediating diverse signaling processes and are promising therapeutic targets for a number of diseases[10,11]. SFKs contain regulatory domains that modulate their catalytic phospho-transfer activity and cellular localization. A number of studies have revealed the structural and biochemical basis of the catalytic regulation of SFKs[12,13]. Despite this extensive characterization, how regulatory domain interactions influence the ability of the ATP-binding pocket to accommodate small-molecule ligands is not well understood. Using our labeling method, we have identified a series of ATP-competitive inhibitors that display distinct selectivity for the active sites of autoinhibited SFKs *in vitro* and *in situ*. Furthermore, by obtaining a structure of one of these inhibitors bound to the catalytic domain of SRC, we have identified the molecular determinants of this preference. Finally, we show that inhibitors that display a preference for autoinhibited SFKs modulate the ability of their regulatory domains to engage in intermolecular interactions. These studies provide insight into how inhibitors can be designed to modulate interactions outside of the ATP-binding site of this therapeutically important enzyme family.

## Results

### A photo-affinity probe for profiling kinase active sites

We identified three necessary components for developing general probes that can be used to profile the functional states of protein kinases in complex protein mixtures: (i) a general ligand that can direct a probe to the active site of protein kinases, (ii) a reactive moiety that allows the covalent labeling of bound kinase active sites, and (iii) a chemo-selective tag for conjugation to a reporter. For our studies, the cancer drug dasatinib was selected as the directing group due to its broad kinase target profile. Chemical proteomics studies have determined that dasatinib targets over 40 kinases, including many of clinical interest[7,14–16]. Furthermore, the interaction of this drug with kinases has been both biochemically and structurally characterized, so it can be derivatized without affecting potency or selectivity[16–18]. In order to allow covalent labeling of bound kinase active sites, the

piperazine moiety of dasatinib was modified with a photo-reactive benzophenone photo-crosslinker (Fig. 1a). Although a number of chemoselective tags can be used to detect labeled kinase targets[19], we wished to develop a method that allows rapid and quantitative determination of crosslinking efficiency in a single experiment using immunoblotting as a readout. To do this, an orthogonal chemical handle hexylchloride, which is able to undergo a rapid and selective reaction with the self-labeling protein HaloTag, was incorporated into our probe (**1**, Fig. 1b)[20]. The ability to selectively conjugate a large protein to labeled kinases allows for photo-crosslinking efficiency to be determined with a ratiometric gel-shift assay (Supplementary Results, Supplementary Fig. 1).

**Labeling protein kinases in lysates and live cells**

Prior to performing labeling reactions with **1**, we determined whether our modifications affected the capacity of dasatinib to interact with its kinase targets. As expected, **1** retained the ability to potently inhibit the kinases that it was tested against (Supplementary Table 1). Next, the crosslinking efficiency of hexylchloride probe **1** was determined using two different sets of reaction conditions. In the pre-conjugation method, **1** is conjugated to the active site of HaloTag prior to performing photo-crosslinking experiments. The HaloTag-1 conjugate, HT-1, is then incubated with a protein mixture and inhibitor-bound kinases are labeled upon irradiation with UV light (Fig. 1c and Supplementary Fig. 2). In the post-conjugation method, **1** is first photo-crosslinked to inhibitor-bound targets and labeled proteins are subsequently conjugated to HaloTag. For both methods, the percentage of labeled kinase can be determined by separating UV-irradiated samples on an SDS-PAGE gel and probing with a kinase-specific antibody. This results in two distinct bands: a band corresponding to the unlabeled kinase and a mass-shifted band corresponding to the crosslinked kinase conjugated to HaloTag (Supplementary Fig. 1). The efficiency of each method was compared by performing crosslinking experiments with recombinant SRC that had been added to mammalian cell lysates (Fig. 1d and Supplementary Fig. 3). At least 50% of SRC was photo-crosslinked when **1** was conjugated to HaloTag prior to UV irradiation (Fig. 1d), with labeling remaining linear for up to 30 minutes (Supplementary Fig. 4). A similar crosslinking efficiency was observed for the SFK HCK. For both kinases, the absence of a higher molecular weight complex in the presence of an excess of active site competitor demonstrates that the crosslinking event is dependent upon active site binding. In contrast, the post-conjugation method was found to give a much lower crosslinking efficiency (Supplementary Fig. 3). Based on these results, all further experiments were carried out with the pre-conjugation method.

We next determined if our probe was able to efficiently label endogenous protein kinases in mammalian cell lysates. The HT-1 conjugate was incubated with COS-7 cell lysate and then irradiated with UV light. Immunoblotting with an $\alpha$-SFK antibody demonstrated that greater than 50% of the endogenous SFKs were labeled. (Fig. 2a) A similar crosslinking efficiency (~30%) was observed in HeLa cell lysate (Fig. 2a). Next, the ability of **1** to label kinases in live cells was explored. COS-7 cells transiently expressing HaloTag were treated with probe **1** (Fig. 2b). After incubation and irradiation, the amount of photo-crosslinked SRC was determined. Under these conditions, a mass-shifted band corresponding to the kinase-HaloTag conjugate was observed. For cells that were also incubated with a competitor, no

crosslinked kinase was observed. Kinase crosslinking in cells was also found to be UV light dependent (Supplementary Fig. 5) and linear with irradiation time (Supplementary Fig. 6). These results demonstrate that **1** is able to efficiently label endogenous kinases in live cells.

The ability of **1** to efficiently label individual nonreceptor tyrosine kinases in cells was next determined. The SFKs SRC, HCK, LCK, FGR, and BLK and the Tec-family kinase BTK were co-transfected with HaloTag into COS-7 cells. HaloTag-expressing cells were incubated with **1**, followed by UV irradiation. Under these conditions, **1** labeled all of the kinases tested (Fig. 2c and Supplementary Fig. 7). Remarkably, 37% and 14% of total intracellular SRC and HCK were labeled by HT-1, respectively. Although LCK, FGR, BLK, and BTK were not labeled as efficiently, the amount of crosslinking observed is sufficient for intracellular profiling of these kinases. The absence of a mass-shifted band for crosslinking experiments performed in the presence of a dasatinib competitor demonstrated that labeling was active site-dependent (Supplementary Fig. 7). Furthermore, introduction of an ATP-binding site mutation, SRC$^{T338I}$, which disrupted dasatinib binding[16], prevented active site labeling (Fig. 2c).

## Profiling multiple SFK activation states

Most protein kinases within the cell possess low catalytic activity in the absence of external stimuli. These enzymes are activated in response to signaling events through a number of mechanisms[12,21]. Activation causes conformational changes that align key catalytic residues in the ATP-binding site. In SFKs, the catalytic activity of the ATP-binding site is controlled by intramolecular regulatory domain interactions[12,13,22]. These multidomain proteins contain SH2 and SH3 regulatory domains at the N terminus and a C-terminal catalytic kinase domain. Intramolecular engagement of the SH2 and SH3 domains clamps the kinase in a catalytically inactive conformation. Release of these intramolecular interactions leads to activation of the catalytic domain. Despite extensive study of these regulatory interactions, it is still unclear how these events affect the conformation of the ATP-binding sites of SFKs.

The active sites of protein kinases can sample multiple conformational states, and a photo-affinity probe that does not rely on catalytic activity has the potential to profile all of them. Therefore, we determined the ability of **1** to profile SFKs across a range of activation states. To this end, a panel of SRC and HCK constructs was assembled. A series of mutations outside the active sites of SRC and HCK were selected; each set of mutations biased these kinases towards a specific activation state (Fig. 3a; SRC residue numbering is used to identify each of the various mutations). Highly activated SRC and HCK constructs, SRC$^{Act}$ and HCK$^{Act}$, contain mutations that disrupt the interaction of the SH2 linker and SH3 domain as well as convert Tyr527 to a nonphosphorylatable phenylalanine. These constructs preclude intramolecular binding and allow the kinase to adopt an activated state[23,24]. SRC and HCK variants of intermediate activity were generated by mutating tyrosine residues that are regulated by phosphorylation to phenylalanines (Y416F or Y527F). Mutating Tyr527 to a phenylalanine (Y527F) considerably weakened SH2-domain binding because the unmodified C-terminal tail is a suboptimal ligand for this domain. Y416F removes the activation loop residue that is phosphorylated in SFKs[25]. In addition, two variants that cause SFKs to adopt a closed conformation, and therefore possess low catalytic activity, were

generated. The SH3 domain-engaged SFK constructs, SRC$^{SH3eng}$ and HCK$^{SH3eng}$, are autoinhibited because the introduction of multiple prolines into the SH2 linker enhances the affinity of the SH3 domain for this segment[26]. The SH2 domain-engaged SFK constructs, SRC$^{SH2eng}$ and HCK$^{SH2eng}$, contain a C-terminal tail that is a high affinity ligand for the SH2 domain independent of Tyr527 phosphorylation[27–30]. Prior to performing labeling experiments, each construct was transiently expressed in COS-7 cells and the level of activation loop phosphorylation was determined with a phospho-Y416-specific antibody (Fig. 3b). The relative amounts of phosphorylation are consistent with the engineered regulatory preferences of these constructs.

The ability of **1** to label the active sites of the constructs described above was determined in COS-7 cells. Photo-crosslinking experiments were performed. Interestingly, **1** labeled each series of SFK constructs with almost equal efficiency, regardless of the activation state (Fig. 3c and Supplementary Fig. 8). All of the SRC constructs were labeled with comparable efficiency (35–45%). The HCK variants followed a similar trend, with a crosslinking efficiency of 11–17%. These results are consistent with a study that demonstrated that dasatinib had a similar affinities for unactivated and activation loop-phosphorylated ABL[31].

## Interrogation of SFK active sites

From previous studies of SFK activity and regulation, it has been established that (i) SFKs adopt several different ATP-binding site conformations and (ii) regulatory domain interactions control the catalytic activity of this kinase family. We sought to examine the interplay between these sites in a physiologically relevant context with **1**. To do this, we assembled a series of ATP-competitive SRC and HCK inhibitors to determine whether any of these ligands displayed a preference for the distinct active or autoinhibited states (Fig. 4a). The capacity of **1** to label multiple activation states with equal efficiency provided us with a means to rapidly profile each inhibitor in a competition assay. Prior to testing our panel of HCK and SRC inhibitors in cells, their abilities to compete with **1** for ATP-binding site labeling was determined with purified SRC and HCK constructs *in vitro*. HCK$^{SH3eng}$, HCK$^{SH2eng}$, and SRC$^{SH2eng}$, which contain intramolecularly engaged regulatory domains, were tested. Activated phospho-isoforms of SRC and HCK, generated via auto-phosphorylation of the activation loop of SRC$^{Y527F}$ and HCK$^{Y527F}$, were also screened (Supplementary Fig. 9). To allow quantitative and rapid determination of crosslinking inhibition, a fluorescently-labeled HT-1 construct was used.

In total, nine SFK inhibitors were profiled against the purified SFK variants described above (Fig. 4a and Table 1). Several of the inhibitors tested (**2**, **8–10**) were more effective competitors of the autoinhibited HCK constructs (HCK$^{SH3eng}$ and HCK$^{SH2eng}$) than activated HCK. A similar trend was observed with inhibitors **8–10** for the SRC variants. Interestingly, several inhibitors displayed divergent effects on SRC and HCK. For example, **3** and **6** more effectively competed for crosslinking to SRC$^{Act}$ than SRC$^{SH2eng}$ but had little preference for any of the HCK variants. Inhibitors based on the pyrazolopyrimidine scaffold (**6–10**) demonstrated some of the most interesting differences in the competition assays for the HCK and SRC constructs (Table 1). Inhibitors that contained smaller aryl substituents at the *C*-3 position of the pyrazolopyrimidine core (**6** and **7**) were almost equally potent

competitors for the activated and autoinhibited SFK variants. In contrast, analogs that contained larger aryl groups at the *C*-3 position (**8–10**) demonstrated a striking preference for autoinhibited SRC and HCK constructs over their activated forms. For example, inhibitor **8** competed 57- and 90-fold more effectively for $HCK^{SH2eng}$ and $HCK^{SH3eng}$ than for activated HCK, respectively. Similarly, inhibitors **9** and **10** showed a distinct preference for the ATP-binding sites of autoinhibited SRC and HCK over $SRC^{Act}$ and $HCK^{Act}$. To confirm these trends, inhibitors **7–10** were tested in an *in vitro* activity assay against activated and autoinhibited SRC and HCK constructs (Supplementary Fig. 10). Consistent with the results of the photo-crosslinking competition experiments, inhibitors **8–10** had significantly lower $K_i$s for the autoinhibited forms of SRC and HCK. Furthermore, **7**, which had a similar $IC_{50}$ for all of the SFK constructs in the photo-crosslinking competition experiments, was an almost equipotent inhibitor of all of the SFK constructs.

To determine whether pyrazolopyrimidine ligands demonstrated the same selectivity trend in a more physiologically relevant environment, cellular competition assays were performed to obtain *in situ* $IC_{50}$ values. To do this, crosslinking experiments were performed in COS-7 cells with variable concentrations of dasatinib or **10** as competitors. Competition experiments were performed with the highly activated SFK constructs, $SRC^{Act}$ and $HCK^{Act}$, and their autoinhibited analogs $SRC^{SH3eng}$ and $HCK^{SH3eng}$. After irradiation, the extent of competition at each inhibitor concentration was determined via immunoblotting (Supplementary Fig. 11). **10** produced the same trend with SRC and HCK *in situ* as it did in the *in vitro* competition experiments. This inhibitor is at least 70-fold more potent in the cellular competition assay against $HCK^{SH3eng}$ over $HCK^{Act}$ (Fig. 4b and Supplementary Fig. 12). In cells, **10** did not show significant competition for $SRC^{Act}$ at the highest concentration tested (3 μM) but competed effectively for the autoinhibited form of SRC ($SRC^{SH3eng}$).

## 9 stabilizes an inactive conformation of SRC

Due to the distinct binding preferences of inhibitors **8–10** for autoinhibited forms of SRC and HCK, we sought to understand how this class of ligands interacts with the ATP-binding sites of SFKs. To this end, we obtained a crystal structure of **9** bound to the catalytic domain of SRC (Fig. 5 and Supplementary Fig. 13). Two molecules of unphosphorylated SRC kinase domain bound to **9** were observed per crystallographic asymmetric unit. As expected, inhibitor **9** occupied the ATP-binding site of SRC, making many of the same interactions as the adenine ring of ATP. Interestingly, the catalytic domain of **9** adopted the SRC/CDK-like inactive conformation[32–34]. This inactive conformation is characterized by movement of helix αC in the *N*-terminal lobe, with the rotation of a conserved, catalytically-important glutamic acid residue (Glu310) (Fig. 5b, c). The chlorobenzyloxy group at the *C*-3 position of the pyrazolopryimidine scaffold projected into the pocket created by the movement of helix αC. Although the chlorobenzyloxy groups adopted slightly different conformations in the two complexes, in both cases an overlay of the inhibitor **9**-SRC complex with a crystal structure of active SRC showed that the bulky aryl group would not be accommodated by the active form of the enzyme (Fig. 5d). Our crystallographic observations show that pyrazolopyrimidine inhibitors with extended substituents at the *C*-3 position stabilize the SRC/CDK-like inactive conformation of SFK ATP-binding sites.

### 8–10 modulate the regulatory domain accessibility of SFKs

Our competition results demonstrate that certain classes of inhibitors have higher affinities for auto-inhibited SRC and HCK constructs, while others do not. Thus, regulatory interactions affect the conformation of SFK active sites. We were curious whether stabilizing the ATP-binding sites of SFKs in a specific conformation would affect the ability of their regulatory domains to engage in intermolecular interactions. Inhibitors **8–10** were tested for their capacity to modulate the intermolecular accessibility of the SH3 domains of SRC and HCK (Supplementary Fig. 14). SH3 domain pull-down experiments with a polyproline (PP) peptide ligand were performed with SRC$^{Y527F}$ and HCK$^{Y527F}$ in the presence of saturating amounts of various inhibitors (Fig. 6a). In the presence of dasatinib, 22% and 27% of SRC$^{Y527F}$ and HCK$^{Y527F}$ were retained on the beads, respectively (Fig. 6b and Supplementary Fig. 15). In contrast, little to no SRC$^{Y527F}$ or HCK$^{Y527F}$ was pulled down when these SFKs were bound to inhibitors **8–10**. Similar amounts of the isolated SH3 domain of HCK were retained on the beads when pull-down experiments were performed in the presence of dasatinib, **9** or **10**, demonstrating that the observed differences in SH3 domain accessibility are due to ATP-binding site interactions (Supplementary Fig. 16). The diminished capacity of the SH3 domains of SRC and HCK to engage in intermolecular interactions when bound to inhibitor **10** was confirmed with a quantitative binding assay (Supplementary Fig. 17). The binding affinities of the SH3 domains of SRC$^{Y527F}$-**10** and HCK$^{Y527F}$-**10** for a fluorescently-labeled PP ligand was at least 10-fold lower than for SRC$^{Y527F}$-dasatinib and HCK$^{Y527F}$-dasatinib. Divergent behavior was observed for inhibitor **2** in the pull-down assay. Consistent with the preference that **2** demonstrates for autoinhibited HCK constructs, the SH3 domain of the HCK$^{Y527F}$-**2** complex was hindered in its ability to engage an intermolecular PP ligand (Fig. 6b and Supplementary Fig. 15). However, when SRC$^{Y527F}$ was bound to **2**, a majority of its SH3 domain was accessible to an intermolecular SH3 ligand, which is consistent with the modest preference that this inhibitor shows in crosslinking competition assays for activated SRC. These pull-down experiments clearly demonstrate that the intermolecular accessibility of SFK regulatory interactions can be modulated through their ATP-binding sites.

## Discussion

In this study, we describe a new method for quantitatively analyzing the ATP-binding site occupancies of protein kinases in cell lysates and live cells. This methodology utilizes a probe, **1**, that can be used to covalently label the active sites of protein kinases. The incorporation of a hexylchloride group allows the efficiency of the photo-crosslinking event to be determined ratiometrically. Although we have applied this methodology to protein kinases, this strategy should be applicable to any small-molecule probe that can be modified with an appropriate linker. This should allow for the development of quantitative labeling tools for the analysis of a number of protein families. The ability to apply **1** to quantitatively and efficiently profile kinase active site accessibility in physiologically relevant environments has proved useful for studying SFKs. Specifically, we determined how regulatory domain interactions influence the conformation of the ATP-binding sites of SRC and HCK. We were able to identify several inhibitors (**8–10**) that were selective for the autoinhibited forms of these SRC and HCK kinases. Although this screen could have been

performed with any method that allows the ATP-binding site occupancies of SFK constructs with variable activation states to be determined, our labeling strategy was particularly well suited for this task.

To determine whether the observed preferences of inhibitors **8–10** for auto-inhibited SRC and HCK variants can be explained by the conformation of their ATP-binding sites when bound to these ligands, we obtained a crystal structure of **9** in complex with the catalytic domain of SRC (Fig. 5a). Interestingly, SRC was in the SRC/CDK-like inactive conformation. This conformation is characterized by the movement and rotation of helix αC in the *N*-terminal lobe of the catalytic domain, which disrupts a salt bridge between Glu310 in helix αC and a conserved catalytic lysine (Lys295) (Fig. 5b). The ATP-binding site of SRC in the SRC-**9** complex is distinct from the inactive form, called the DFG-out conformation, that the tyrosine kinase ABL adopts when bound to the drug imatinib[35]. With one exception, all previous structures of isolated SFK catalytic domains have been in either the active or the DFG-out conformation[32,36–38]. Generally, the SRC/CDK-like inactive conformation has only been observed in autoinhibited SFK constructs that contain SH2 and SH3 regulatory domains[33,34].

The SRC/CDK-like conformation has been observed for a number of kinases[21]. For example, the receptor tyrosine kinase EGFR adopts the SRC/CDK-like inactive conformation when bound to the drug lapatinib[39]. Directly relevant to our observations, the kinase domain of Bruton's tyrosine kinase (BTK) displays ligand-induced conformational changes when bound to pyrazolopyrimidine inhibitor **10** and the ATP-binding site is in the SRC/CDK-like conformation[40]. Superposition of BTK bound to **10** and SRC bound to **9** showed that their ATP-binding sites are nearly identical in the presence of these inhibitors, with helix αC undergoing a similar degree of movement and rotation (Supplementary Fig. 18a). Inhibitor **10** would not be accommodated in the active form of BTK without this movement. Superposition of inhibitor **10** with the active form of SRC shows that a similar steric clash would be predicted to occur with helix αC (Supplementary Fig. 18b).

We hypothesized that stabilizing the SRC/CDK-like inactive conformation of SRC and HCK with ATP-competitive inhibitors would influence their regulatory domains. Consistent with our speculation, there was a direct correlation between an inhibitor's preference for autoinhibited SFK constructs and its ability to induce an inaccessible SH3 domain. Inhibitors **8–10** hinder the intermolecular interactions between the SH3 domains of these kinases with a PP peptide ligand. Presumably this occurs because the SH3 domain's intramolecular interaction with the SH2 linker is strengthened. These results show that ATP-competitive inhibitors that stabilize the ATP-binding site in distinct conformations influence distal regulatory domains.

These results have direct implications for the pharmacological inhibition of multidomain protein kinases like the SFKs. Many multidomain protein kinases use their regulatory domains to engage other signaling partners in the cell, often recruiting their catalytic domains to activated signaling complexes. Inhibitors, like **8–10**, that stabilize an inactive ATP-binding site conformation and promote the intramolecular engagement of regulatory interactions would be predicted to prevent kinases from being recruited to active signaling

complexes. This is in contrast to several recently reported examples of ATP-competitive kinase inhibitors that lead to activation or priming of specific signaling pathways[41–43]. Furthermore, while kinase phospho-transfer activity is essential for a variety of cellular processes, growing evidence suggests that these enzymes possess a number of important noncatalytic functions[44]. Protein kinases mediate protein scaffolding complexes, allosterically regulate other enzymes, and modulate protein-protein and protein-DNA interactions through mechanisms independent of their enzymatic activity. For example, the SH2 and SH3 domains of SRC allow this kinase to play important noncatalytic functions in integrin signaling and the formation of focal adhesions[45]. In SRC-deficient fibroblasts, kinase dead SRC mutants can rescue cell spreading on fibronectin to comparable levels as the wild-type protein. SFKs have also been shown to have other noncatalytic roles in JAK2 signaling, antigen-specific T-cell activation, and in B-cell antigen receptor signaling[46–48]. Beyond the SFKs, a large number of protein kinases contain additional domains that play important roles in both the catalytic and noncatalytic functions of these enzymes. The use of conformation-specific ATP-competitive inhibitors provides the opportunity to control the noncatalytic functions of protein kinases by modulating their abilities to engage in intermolecular protein-protein interactions. Thus, it may be possible to obtain different phenotypic effects through the ATP-competitive inhibition of the same kinase, simply by varying how an inhibitor interacts with the ATP-binding site. Finally, ATP-competitive inhibitors that modulate interactions outside of kinase active sites may allow for the differential regulation of the large number of pseudokinases, which are predicted to lack catalytic activity, encoded by the human genome.[49] Chemical proteomic tools similar to those described in this study should aid in the discovery of pharmacological agents with these interesting properties.

## Methods

Synthesis and characterization of probes are described in the Supplementary Methods.

### SFK construct expression and purification

SRC-family kinases SRC (residues 84–533) and HCK (residues 84–531) were expressed and purified as previously described[50]. Mutations were introduced into SRC and HCK by site-directed mutagenesis and were verified by DNA sequencing. SFK[Act] variants contained the following mutations (SRC residue numbering is used to identify each of the various mutations): SRC (K249E/P250E/Y527F) and HCK (P250A/P253A/Y527F). SFK[SH3eng] variants contained the following mutations: SRC (K249P/Q252P/T253P) and HCK (K249P/K252P). SFK[SH2eng] variants contained the following mutations: SRC (Q528E/P529E/G530I) and HCK (Q528E/Q529E/Q530I). Mutant SRC and HCK constructs were expressed and purified following the same procedure.

### General procedure for *in vitro* photo-labeling of recombinant kinases with probe 1

Purified kinase (100 nM), mammalian lysate (0.5 mg/ml) and HT-**1** (500 nM) were diluted in PBS in a 96-well, U-bottom plate. Samples were prepared either in the absence or presence of 10 µM dasatinib. Samples were mixed and irradiated on ice at 365 nm for 30 minutes by placing a Spectroline ENF-260C UV lamp directly on top of the plate. After

irradiation, 25 μL of 3X SDS loading buffer was added. Samples were separated by SDS-PAGE and visualized via Western blot using a non-phospho-SFK (Tyr416) (7G9) antibody (Cell Signaling). The scanned blots were quantified with LI-COR Odyssey software (mean ± SEM, n = 3). To determine the percent kinase crosslinked, the intensities of the mass-shifted band and the non-crosslinked kinase were measured. After background correction, the amount of crosslinked protein was calculated as the percentage of mass-shifted kinase over the amount of total kinase (sum of the mass-shifted and non-crosslinked kinase signals).

### *In vitro* competition assays with SFK variants using ATP-competitive SFK inhibitors

Purified kinase (25 nM), mammalian lysate (0.2 mg/ml), and HT-**1** (150 nM) were diluted in PBS in a 96-well, U-bottom plate. The ATP-competitive inhibitor (3-fold dilutions over 9 wells) was added to the kinase mixture, and the plate was incubated at room temperature for 20 minutes prior to photo-crosslinking. Samples were mixed and irradiated on ice at 365 nm for 30 minutes by placing a Spectroline ENF-260C UV lamp directly on top of the plate. After irradiation, DTT (1 mM) and a fluorescein-tag (500 nM) were added. Samples were incubated at room temperature in the dark for one hour and quenched with 25 μl of 3X SDS loading buffer. Samples were separated by SDS-PAGE and visualized via in-gel fluorescence scanning using a GE Typhoon FLA 9000. The intensities of the mass shifted bands at each inhibitor concentration were quantified with ImageQuant. Data was analyzed using Prism Graphpad software and $IC_{50}$ values were determined using non-linear regression analysis (mean ± SEM, n = 3). Inhibitors that were found to have an $IC_{50}$ less than 25 nM were re-tested at lower concentrations of SRC and HCK.

### *In situ* labeling of SFK variants with probe 1

All cells were grown at 37°C in high glucose DMEM supplemented with 10% FBS and streptomycin/penicillin. Cell culture protocol is detailed in the Supplementary Methods. COS-7 cells, grown in a 12-well plate, were co-transfected with a HaloTag fusion construct (pDest26) and the kinase of interest (pcDNA3.2-V5) using Fugene HD reagent (Promega). The cells were incubated at 37°C for 24 hours. The transfected cells were treated with 1 μM of **1** in 1 ml of media (high glucose DMEM, 10% FBS with Strep/Pen) for one hour at 37°C. The cells were then washed with media (3×, 5 minutes at 37°C) and then 1 ml of PBS was added. The cells were irradiated at 365 nm at 37°C for eight minutes by placing a Spectroline ENF-260C UV lamp directly on top of the uncovered plate. After irradiation, the PBS was aspirated and the cells were lysed with 1X SDS loading buffer containing PhosStop phosphatase inhibitor (Roche). Samples were separated on an SDS-PAGE gel and visualized via Western blot using an anti-V5 tag antibody (Sigma). The scanned blots were quantified with LI-COR Odyssey software to determine crosslinking efficiency (mean ± SEM, n = 3).

### Pull-down assay to determine SH3 domain accessibility

*Formation of kinase-inhibitor complex*: The kinase of interest (100 nM) and mammalian lysate (0.2 mg/ml) were diluted in immobilization buffer (50 mM Tris, 100 mM NaCl, 1 mM DTT, pH 7). The inhibitor of interest (5 μM) was added to this kinase dilution. DMSO was added to those samples that used no inhibitor. The mixture was allowed to incubate for

30 minutes prior to loading on the resin. *Pull-down*: 40 μl of a 50% slurry of SNAP-Capture Pull-down Resin (NEB) was placed in a microcentrifuge tube. The resin was washed (2×, 10 bed volumes) with immobilization buffer. A SNAP-tag-polyproline (PP) peptide fusion (VSLARRPLPPLP) (10 μM) was loaded onto the resin at a final volume of 100 μL in buffer. The resin was shaken at room temperature for 90 minutes, with agitation by a pipet every 15 minutes. After PP peptide immobilization, the resin was washed (2×, 10 bed volumes) and 100 μL of the kinase-inhibitor complex was loaded. The resin was allowed to shake at room temperature for one hour. After incubation with the kinase-inhibitor complex, the flow-through was collected and the resin washed (4×, 10 bed volumes). To elute the retained kinase, 100 μL of 1X SDS loading buffer was added and the beads were boiled at 90°C for 10 minutes. All samples were separated by SDS-PAGE and visualized via Western blot using an anti-His6 antibody (abm). The scanned blots were quantified with LI-COR Odyssey software to determine percent kinase retained on the resin based on the loaded and eluted fractions (mean ± SEM, n = 3).

## Statistical analysis

All experiments were performed in triplicate, unless otherwise specified. Results are shown as mean ± standard error of the mean (SEM). Error bars represent ± SEM.

## Supplementary Material

Refer to Web version on PubMed Central for supplementary material.

## Acknowledgements

## References

1. Manning G, Whyte DB, Martinez R, Hunter T, Sudarsanam S. The protein kinase complement of the human genome. Science. 2002; 298:1912–1934. [PubMed: 12471243]

2. Cohen P. Protein kinases – the major drug targets of the twenty-first century? Nat. Rev. Drug Discovery. 2002; 1:309–315. [PubMed: 12120282]

3. Zhang J, Yang PL, Gray NS. Targeting cancer with small molecule kinase inhibitors. Nat. Rev. Cancer. 2009; 9:28–39. [PubMed: 19104514]

4. Cravatt BF, Wright AT, Kozarich JW. Activity-based protein profiling: from enzyme chemistry to proteomic chemistry. Annu. Rev. Biochem. 2008; 77:383–313. [PubMed: 18366325]

5. Barglow KT, Cravatt BF. Activity-based protein profiling for the functional annotation of enzymes. Nat. Methods. 2007; 4:822–827. [PubMed: 17901872]

6. Simon GM, Cravatt BF. Activity-based proteomics of enzyme superfamilies: serine hydrolases as a case study. J. Biol. Chem. 2010; 285:11051–11055. [PubMed: 20147750]

7. Bantscheff M, et al. Quantitative chemical proteomics reveals mechanisms of action of clinical ABL kinase inhibitors. Nat. Biotechnol. 2007; 25:1035–1044. [PubMed: 17721511]

8. Patricelli MP, et al. In situ kinase profiling reveals functionally relevant properties of native kinases. Chem. Biol. 2011; 18:699–710. [PubMed: 21700206]

9. Sharma K, et al. Proteomics strategy for quantitative protein interaction profiling in cell extracts. Nat. Methods. 2009; 6:741–744. [PubMed: 19749761]

10. Cheng HC, et al. Allosteric networks governing regulation and catalysis of Src-family protein tyrosine kinases: implications for disease-associated kinases. Clin. Exp. Pharmacol. Physiol. 2010; 37:93–101. [PubMed: 19566834]

11. Kim LC, Song L, Haura EB. Src kinases as therapeutic targets for cancer. Nat. Rev. Clin. Oncol. 2009; 6:587–595. [PubMed: 19787002]

12. Huse M, Kuriyan J. The conformational plasticity of protein kinases. Cell. 2002; 109:275–282. [PubMed: 12015977]

13. Boggon TJ, Eck MJ. Structure and regulation of Src family kinases. Oncogene. 2004; 23:7918–7927. [PubMed: 15489910]

14. Karaman MW, et al. A quantitative analysis of kinase inhibitor selectivity. Nat. Biotechnol. 2008; 26:127–132. [PubMed: 18183025]

15. Hantschel O, Rix U, Superti-Furga G. Target spectrum of the BCR-ABL inhibitors imatinib, nilotinib and dasatinib. Leuk. Lymphoma. 2008; 49:615–619. [PubMed: 18398720]

16. Li J, et al. A chemical and phosphoproteomic characterization of dasatinib action in lung cancer. Nat. Chem. Biol. 2010; 6:291–299. [PubMed: 20190765]

17. Shi H, Zhang CJ, Chen GY, Yao SQ. Cell-based proteome profiling of potential dasatinib targets by use of affinity-based probes. J. Am. Chem. Soc. 2012; 134:3001–3014. [PubMed: 22242683]

18. Getlik M, et al. Hybrid compound design to overcome the gatekeeper T338M mutation in cSrc. J. Med. Chem. 2009; 52:3915–3926. [PubMed: 19462975]

19. Best MD. Click chemistry and bioorthogonal reactions: unprecedented selectivity in the labeling of biological molecules. Biochemistry. 2009; 48:6571–6584. [PubMed: 19485420]

20. Los GV, et al. HaloTag: a novel protein labeling technology for cell imaging and protein analysis. ACS Chem. Biol. 2008; 3:373–382. [PubMed: 18533659]

21. Jura N, et al. Catalytic control in the EGF receptor and its connection to general kinase regulatory mechanisms. Mol. Cell. 2011; 42:9–22. [PubMed: 21474065]

22. Engen JR, et al. Structure and dynamic regulation of Src-family kinases. Cell. Mol. Life Sci. 2008; 65:3058–3073. [PubMed: 18563293]

23. Briggs SD, Smithgall TE. SH2-kinase linker mutations release Hck tyrosine kinase and transforming activities in Rat-2 fibroblasts. J. Biol. Chem. 1999; 274:26579–26583. [PubMed: 10473622]

24. Gonfloni S, Frischknecht F, Way M, Superti-Furga G. Leucine 255 of Src couples intramolecular interactions to inhibition of catalysis. Nat. Struct. Biol. 1999; 6:760–764. [PubMed: 10426955]

25. Osusky M, Taylor SJ, Shalloway D. Autophosphorylation of purified c-Src at its primary negative regulation site. J. Biol. Chem. 1995; 270:25729–25732. [PubMed: 7592753]

26. Lerner EC, et al. Activation of the Src family kinase Hck without SH3-linker release. J. Biol. Chem. 2005; 280:40832–40837. [PubMed: 16210316]

27. Alvarado JJ, Betts L, Moroco JA, Smithgall TE, Yeh JI. Crystal structure of the Src family kinase Hck SH3-SH2 linker regulatory region supports an SH3-dominant activation mechanism. J. Biol. Chem. 2010; 285:35455–35461. [PubMed: 20810664]

28. Ayrapetov MK, et al. Conformational basis for SH2-TyRP)527 binding in Src inactivation. J. Biol. Chem. 2006; 281:23776–23784. [PubMed: 16790421]

29. Lerner EC, Smithgall TE. SH3-dependent stimulation of Src-family kinase autophosphorylation without tail release from the SH2 domain in vivo. Nat. Struct. Biol. 2002; 9:365–369. [PubMed: 11976726]

30. Moarefi I, et al. Activation of the Src-family tyrosine kinase Hck by SH3 domain displacement. Nature. 1997; 385:650–653. [PubMed: 9024665]

31. Wodicka LM, et al. Activation state-dependent binding of small molecule kinase inhibitors: structural insights from biochemistry. Chem. Biol. 2010; 17:1241–1249. [PubMed: 21095574]

32. Georghiou G, Kleiner RE, Pulkoski-Gross M, Liu DR, Seeliger MA. Highly specific, bisubstrate-competitive Src inhibitors from DNA-templated macrocycles. Nat. Chem. Biol. 2012; 8:366–374. [PubMed: 22344177]

33. Sicheri F, Moarefi I, Kuriyan J. Crystal structure of the Src family tyrosine kinase Hck. Nature. 1997; 385:602–609. [PubMed: 9024658]

34. Xu W, Harrison SC, Eck MJ. Three-dimensional structure of the tyrosine kinase c-Src. Nature. 1997; 385:595–602. [PubMed: 9024657]

35. Schindler T, et al. Structural mechanism for STI-571 inhibition of abelson tyrosine kinase. Science. 2000; 289:1938–1942. [PubMed: 10988075]

36. Seeliger MA, et al. Equally potent inhibition of c-Src and Abl by compounds that recognize inactive kinase conformations. Cancer Res. 2009; 69:2384–2392. [PubMed: 19276351]

37. Dar AC, Lopez MS, Shokat KM. Small molecule recognition of c-Src via the Imatinib-binding conformation. Chem. Biol. 2008; 15:1015–1022. [PubMed: 18940662]

38. Simard JR, et al. A new screening assay for allosteric inhibitors of cSrc. Nat Chem Biol. 2009; 6:394–396. [PubMed: 19396179]

39. Wood ER, et al. A unique structure for epidermal growth factor receptor bound to GW572016 (Lapatinib): relationships among protein conformation, inhibitor off-rate, and receptor activity in tumor cells. Cancer Res. 2004; 64:6652–6659. [PubMed: 15374980]

40. Marcotte DJ, et al. Structures of human Bruton's tyrosine kinase in active and inactive conformations suggest a mechanism of activation for TEC family kinases. Protein Sci. 2010; 19:429–439. [PubMed: 20052711]

41. Okuzumi T, et al. Inhibitor hijacking of Akt activation. Nat. Chem. Biol. 2009; 5:484–493. [PubMed: 19465931]

42. Poulikakos PI, Zhang C, Bollag G, Shokat KM, Rosen N. RAF inhibitors transactivate RAF dimers and ERK signalling in cells with wild-type BRAF. Nature. 2010; 464:427–430. [PubMed: 20179705]

43. Hatzivassiliou G, et al. RAF inhibitors prime wild-type RAF to activate the MAPK pathway and enhance growth. Nature. 2010; 464:431–435. [PubMed: 20130576]

44. Rauch J, Volinsky N, Romano D, Kolch W. The secret life of kinases: functions beyond catalysis. Cell Commun. Signal. 2011; 9:23. [PubMed: 22035226]

45. Kaplan KB, Swedlow JR, Morgan DO, Varmus HE. c-Src enhances the spreading of src–/– fibroblasts on fibronectin by a kinase-independent mechanism. Genes Dev. 1995; 9:1505–15017. [PubMed: 7541382]

46. Garcia-Martinez JM, et al. A non-catalytic function of the Src family tyrosine kinases controls prolactin-induced Jak2 signaling. Cell Signal. 2010; 22:415–426. [PubMed: 19892015]

47. Katsuta H, Tsuji S, Niho Y, Kurosaki T, Kitamura D. Lyn-mediated down-regulation of B cell antigen receptor signaling: inhibition of protein kinase C activation by Lyn in a kinase-independent fashion. J. Immunol. 1998; 160:1547–1551. [PubMed: 9469408]

48. Xu H, Littman DR. A kinase-independent function of Lck in potentiating antigen-specific T cell activation. Cell. 1993; 74:633–643. [PubMed: 8358792]

49. Boudeau J, Miranda-Saavedra D, Barton GJ, Alessi DR. Emerging roles of pseudokinases. Trends Cell Biol. 2006; 16:443–452. [PubMed: 16879967]

50. Seeliger MA, et al. High yield bacterial expression of active c-Abl and c-Src tyrosine kinases. Protein Sci. 2005; 14:3135–3139. [PubMed: 16260764]
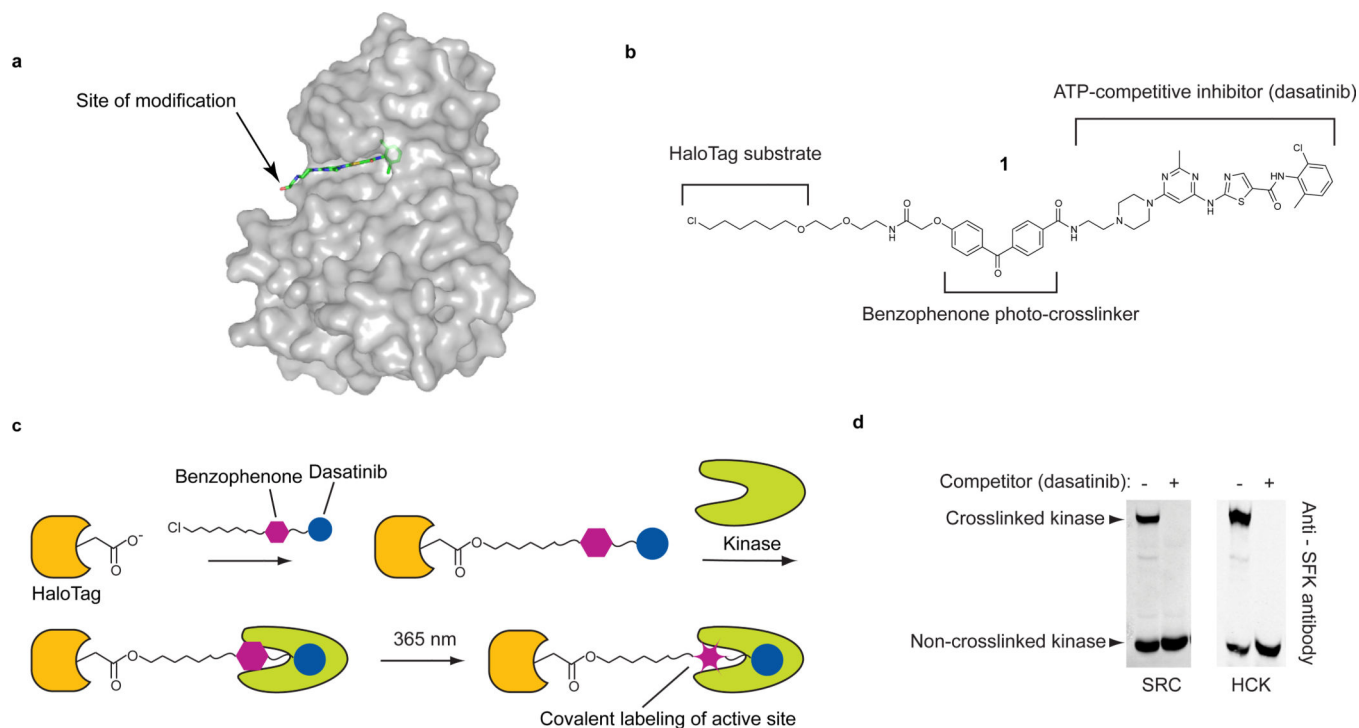
**Figure 1. An active-site directed probe for ratiometric profiling of protein kinases**
(**a**) The cancer drug dasatinib in complex with the tyrosine kinase SRC (PDB code 3G5D).
The arrow shows the site where dasatinib was modified with a benzophenone photo-
crosslinker and an orthogonal chemical tag. (**b**) The chemical structure of probe **1**. Probe **1**
contains three components: (i) a potent ATP-competitive inhibitor (dasatanib), (ii) a photo-
reactive benzophenone crosslinker, and (iii) a hexylchloride tag that selectively labels the
active site of the self-labeling protein HaloTag. (**c**) Experimental crosslinking schematic
using **1**. Prior to photo-crosslinking experiments, HaloTag is labeled with **1**. HT-1 is
incubated with a kinase target and then irradiated with UV light. (**d**). HT-1 efficiently labels
the recombinant SRC-family kinases (SFKs) SRC and HCK in cell lysate. Purified SRC or
HCK (100 nM) was photo-crosslinked with HT-1 in mammalian cell lysate. Immunoblotting
with an anti-SFK antibody shows that a large percentage of SRC and HCK are covalently
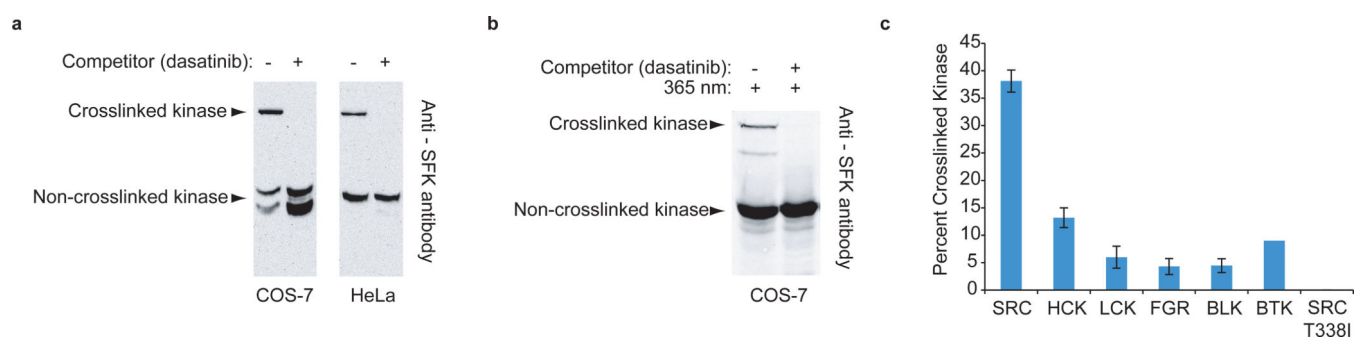modified. Upon addition of a dasatinib competitor, no mass-shifted kinases are observed.

**Figure 2. Characterization of 1 in cell lysate and live cells**

(**a**) HT-1 labels endogenous SFKs in cell lysates. Immunoblots with an anti-SFK antibody are shown for photo-crosslinking experiments performed with COS-7 and HeLa cell lysates. (**b**) Endogenous SFKs in live cells transiently expressing HaloTag are photo-crosslinked by **1**. COS-7 cells transiently expressing HaloTag were treated with **1** and then irradiated with UV light. Immunoblotting with an anti-SFK antibody shows the presence of mass-shifted SFKs. Addition of an active site competitor prevents photo-crosslinking. (**c**) **1** labels nonreceptor tyrosine kinases in live cells. V5-tagged nonreceptor tyrosine kinases were coexpressed with HaloTag in COS-7 cells. After photo-crosslinking, the percent crosslinked kinase was determined with an anti-V5 antibody (mean ± SEM, n = 3).
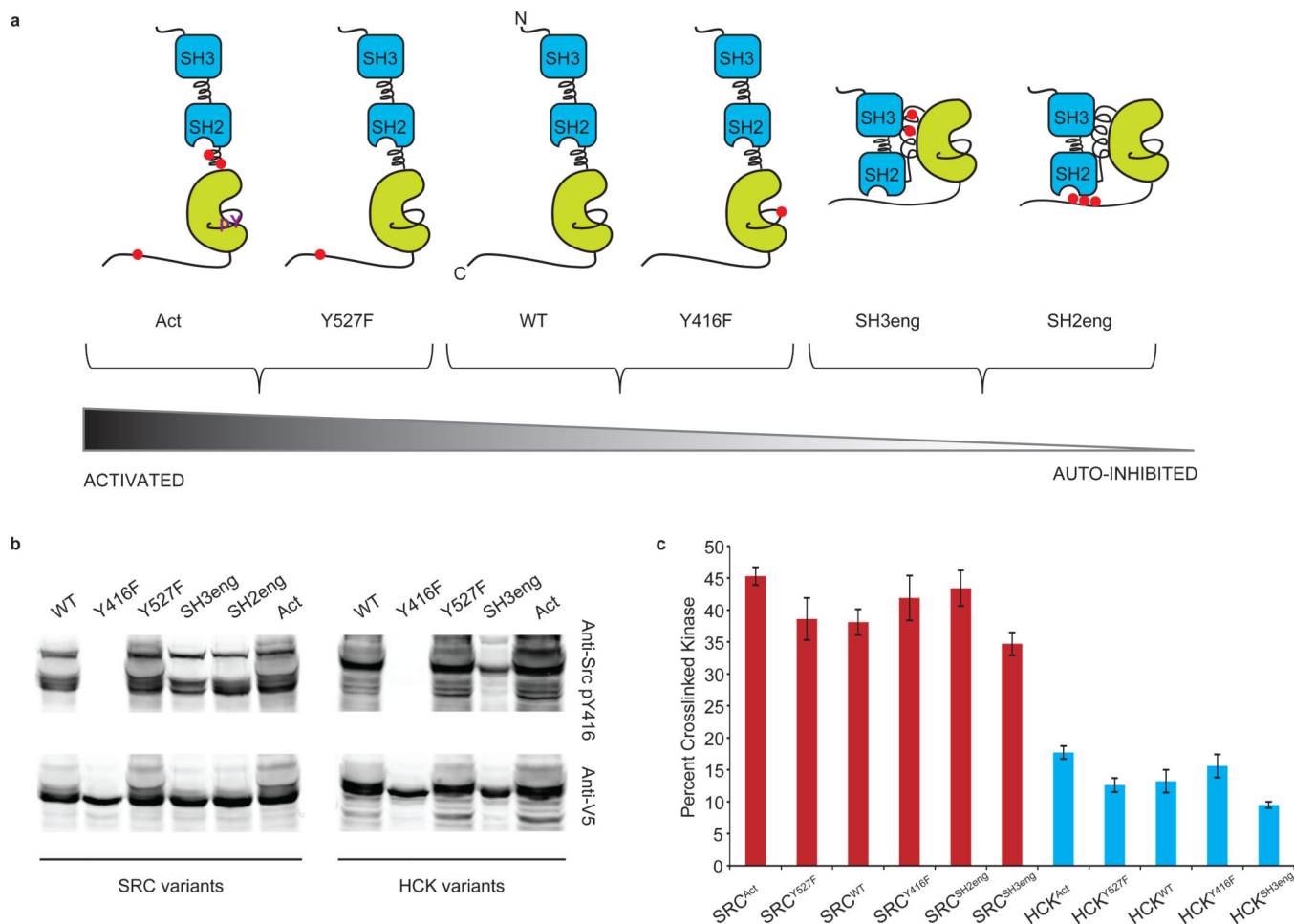
**Figure 3. Photo-crosslinking to SFKs that have diverse regulatory domain interactions**
(**a**) The panel of SRC and HCK variants that was generated in this study. Mutations outside
the active sites of SRC and HCK were introduced to obtain SFKs with diverse regulatory
interactions. Red dots indicate the sites that were modified. (**b**) The activation loop
phosphorylation levels of SFK variants are consistent with their regulatory states. V5-tagged
SRC and HCK constructs were transiently expressed in COS-7 cells and the level of
activation loop phosphorylation (Tyr416) was determined with an anti-phosphoY416-SFK
antibody (phospho-SFK (Tyr416), Cell Signaling). The same samples were immunoblotted
with an anti-V5 antibody. (**c**) **1** labels SFKs with diverse regulatory domain interactions in
live cells (mean ± SEM, n = 3). The regulatory states of SFKs have little effect on overall
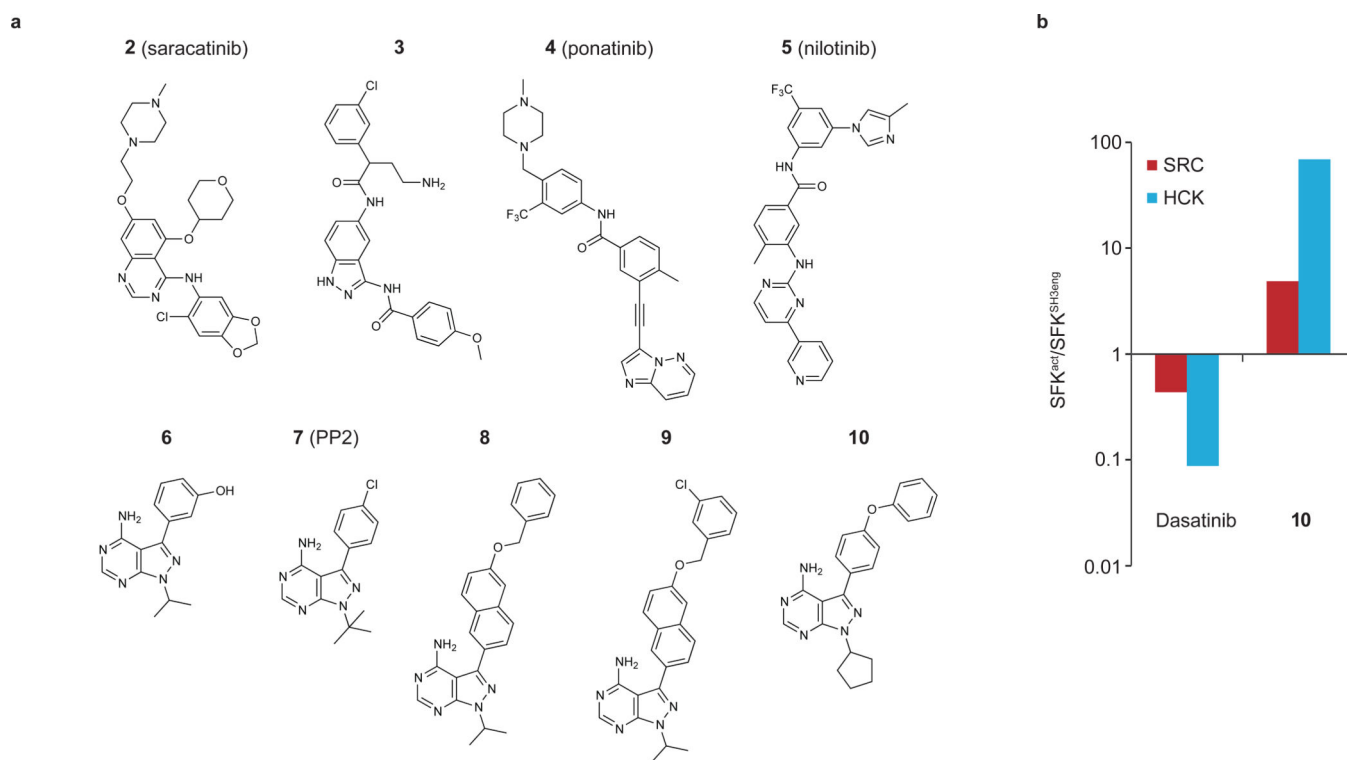photo-crosslinking efficiency.

**Figure 4. Photo-crosslinking competition assays**

(**a**) Chemical structures of the ATP-competitive SFK inhibitors used in photo-crosslinking competition assays with **1**. The IC$_{50}$ values obtained for these inhibitors in photo-crosslinking competition assays with HT-1 and purified SFK constructs are shown in Table 1. (**b**) Quantitative comparison of the fold differences in cellular competition between activated SFK variants (SRC$^{Act}$ and HCK$^{Act}$) and their respective SH3eng constructs (SRC$^{SH3eng}$ and HCK$^{SH3eng}$) for dasatinib and **10**.
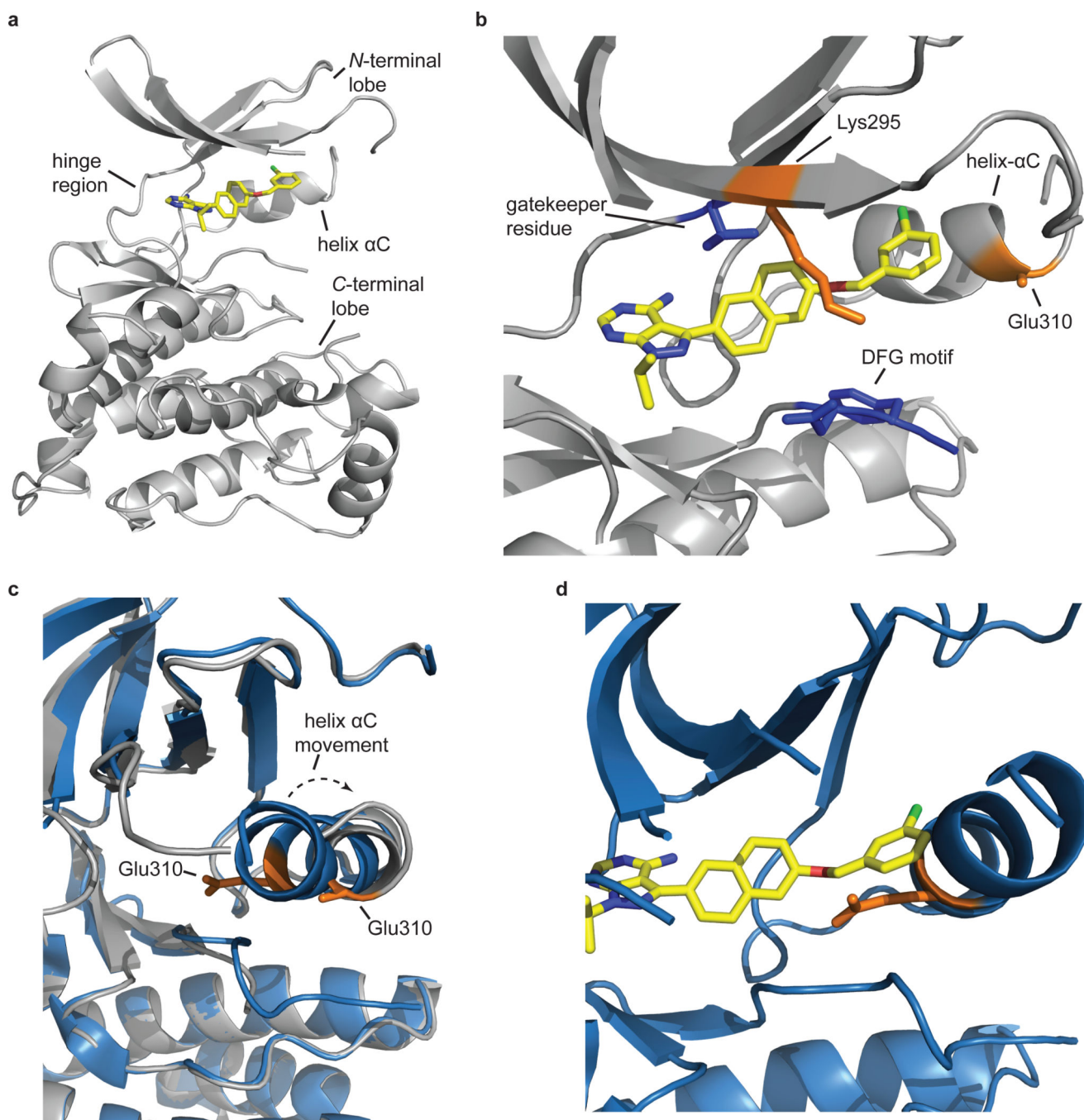
**Figure 5. The catalytic domain of SRC is in the SRC/Cdk-like inactive conformation when bound to 9**

(**a**) Inhibitor **9** (yellow) occupies the ATP-binding site of the catalytic domain of SRC (gray). The pyrazolopyrimidine core sits in the adenine-binding site and makes hydrogen-bonding interactions with the hinge region. (**b**) The naphthyl-benzyloxy substituent displayed from the *C*-3 position sits next to the gatekeeper residue (blue) and projects towards helix αC. Helix αC is rotated outwards from the ATP-binding site relative to its position in the active conformation of SRC, which disrupts a salt bridge between the

catalytic lysine (Lys295) and Glu310 (both shown in orange). Residues 258–276 have been removed for clarity. (**c**) Comparison of the relative positions of the helix αCs in the SRC-**9** complex (gray) and the active form of SRC (SRC-dasatinib (PDB code 3G5D) (blue)). Helix αC moves approximately 4.5 Å in the SRC-**9** complex relative to SRC's helix αC when bound to dasatinib. The rotation and movement of helix αC displaces a conserved glutamic acid residue (Glu 310; shown in orange) that is important for catalysis, which places SRC in the SRC/Cdk-like inactive conformation. (**d**) The benzyloxy group of **9** cannot be accommodated in the active form of SRC. Superposition of **9** with SRC in the active conformation (SRC-dasatinib (PDB code 3G5D)) shows a clear steric clash with helix αC.
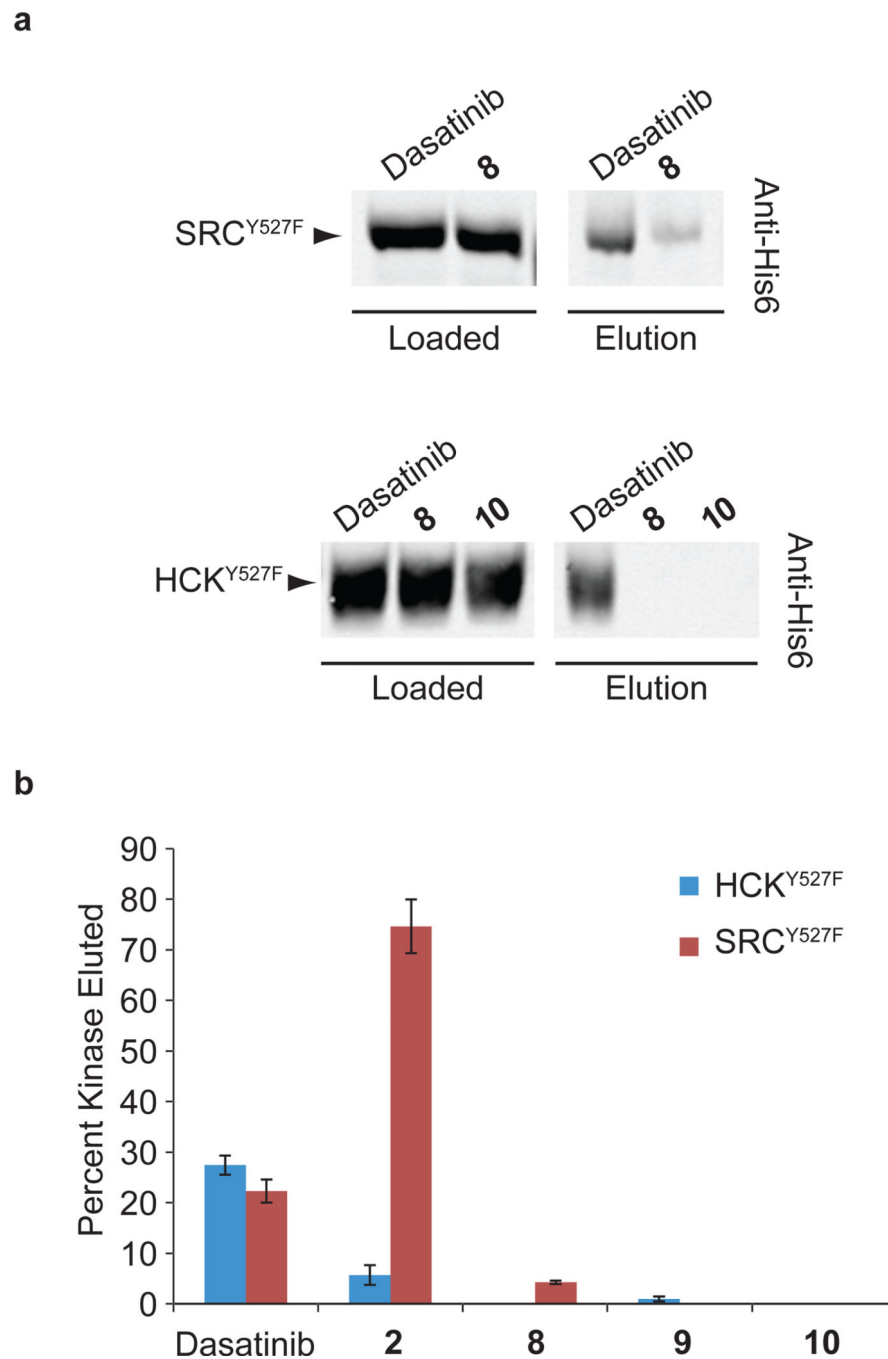
**a**



**b**



**Figure 6. ATP-competitive SFK inhibitors modulate the SH3 domain accessibilities of SRC and HCK**

(**a**) Representative Western blots for pull-down experiments performed with purified SRC$^{Y527F}$ and HCK$^{Y527F}$ in the presence of saturating concentrations of various inhibitors. Loaded samples and resin-eluted samples were immunoblotted using an anti-His6 antibody to determine the percentage of loaded kinase that was retained on the PP ligand-containing beads. (**b**) Quantitation of the pull-down assays performed with SRC$^{Y527F}$ and HCK$^{Y527F}$ in

the presence of each inhibitor that was tested (mean ± SEM, n = 3). The percent of loaded kinase that was eluted from the beads is shown.

**Table 1**

$IC_{50}$ values (nM) for *in vitro* competition assays performed with HT-1 and ATP-competitive inhibitors **2–10** against SRC and HCK variants.

| Compound | Activated SRC* | SRC^SH2eng | Activated HCK* | HCK^SH2eng | HCK^SH3eng |
|---|---|---|---|---|---|
| **Dasatinib** | < 25 | < 25 | < 25 | < 20 | < 1 |
| **2** | 42 ± 15 | 70 ± 9 | 440 ± 120 | 54 ± 7 | 39 ± 1 |
| **3** | 270 ± 50 | 1900 ± 300 | 2100 ± 700 | 3100 ± 300 | 400 ± 100 |
| **4** | 14 ± 2 | 26 ± 1 | 81 ± 8 | 37 ± 11 | 33 ± 11 |
| **5** | > 10000 | > 10000 | > 10000 | > 10000 | 1300 ± 300 |
| **6** | 64 ± 13 | 390 ± 20 | 450 ± 40 | 550 ± 60 | 310 ± 50 |
| **7** | 110 ± 10 | 74 ± 10 | 87 ± 14 | 46 ± 10 | 110 ± 80 |
| **8** | 270 ± 70 | 35 ± 4 | 1100 ± 100 | < 20 | 13 ± 3 |
| **9** | 800 ± 160 | 180 ± 70 | 2700 ± 40 | 63 ± 9 | 27 ± 10 |
| **10** | 1100 ± 500 | < 25 | 490 ± 170 | 27 ± 4 | < 1 |

*
Activated SRC and Activated HCK were obtained via autophosphorylation of the activation loop of SRC[Y527F] and HCK[Y527F].

All IC50 values were determined using the competition assay protocol described in the **Methods** section. All experiments were performed in triplicate, and data represent mean values ± SEM.